Received: 23 February 2019 | Revised: 12 April 2019 | Accepted: 12 April 2019

DOI: 10.1002/rth2.12211

ORIGINAL ARTICLE

rpth research & practice in thrombosis & haemostasis

Crystal structure, epitope, and functional impact of an antibody against a superactive FVIIa provide insights into allosteric mechanism

Longguang Jiang PhD[1] | Xie Xie[1] | Jinyu Li PhD[1] | Egon Persson PhD[2] | Mingdong Huang PhD[1,3]

[1]College of Chemistry, National & Local Joint Biomedical Engineering Research Center on Photodynamic Technologies, Fuzhou University, Fuzhou, China

[2]Haemophilia Biology, Novo Nordisk A/S, Novo Nordisk Park, Måløv, Denmark

[3]Fujian Institute of Research on the Structure of Matter, Chinese Academy of Sciences, Fuzhou, China

Correspondence
Egon Persson, Haemophilia Biology, Novo Nordisk A/S, Novo Nordisk Park, Måløv, Denmark.
Emails: egpe@novonordisk.com; egonrobertpersson@gmail.com
Mingdong Huang, College of Chemistry, National & Local Joint Biomedical Engineering Research Center on Photodynamic Technologies, Fuzhou University, Fuzhou, 350116, China.
Email: HMD_lab@fzu.edu.cn

Funding information
Novo Nordisk-Chinese Academy of Science Research Foundation, Grant/Award Number: NNCAS-2012-5(A); Natural Science Foundation of Fujian Province, Grant/Award Number: 2018J01729; Ministry of Science and Technology of the People's Republic of China, Grant/Award Number: 2017YFE0103200; National Natural Science Foundation of China, Grant/Award Number: 31161130356, 31170707, 31370737 and 31400637; National Key R&D Program of China, Grant/Award Number: 2017YFE0103200

Abstract

Background: Blood coagulation factor VIIa (FVIIa) plays its critical physiological role in the initiation of hemostasis. Even so, recombinant FVIIa is successfully used as a bypassing agent for factor VIII or IX in the treatment of bleeds in patients with severe hemophilia with inhibitors. To investigate the utility of more potent FVIIa variants with enhanced intrinsic activity, molecules such as V21D/E154V/M156Q-FVIIa ($FVIIa_{DVQ}$) were designed.

Methods: Surface plasmon resonance was used to characterize the binding of mAb4F5 to $FVIIa_{DVQ}$ and related variants. X-ray crystallography was used to determine the structure of the Fab fragment of mAb4F5 (Fab4F5). Molecular docking and small-angle X-ray scattering led to a model of $FVIIa_{DVQ}$:Fab4F5 complex.

Results: The binding experiments, functional effects on $FVIIa_{DVQ}$ and structure of mAb4F5 (originally intended for quantification of $FVIIa_{DVQ}$ in samples containing FVII(a)) pinpointed the epitope (crucial role for residue Asp21) and shed light on the role of the N-terminus of the protease domain in FVIIa allostery. The potential antigen-combining sites are composed of 1 hydrophobic and 1 negatively charged pocket formed by 6 complementarity-determining region (CDR) loops. Structural analysis of Fab4F5 shows that the epitope interacts with the periphery of the hydrophobic pocket and provides insights into the molecular basis of mAb4F5 recognition and tight binding of $FVIIa_{DVQ}$.

Conclusion: The binary complex explains and supports the selectivity and functional consequences of Fab4F5 association with $FVIIa_{DVQ}$ and illustrates the potentially unique antigenicity of this FVIIa variant. This will be useful in the design of less immunogenic variants.

KEYWORDS
antibody, blood coagulation, hemophilia, crystal structure, factor VIIa, small-angle X-ray scattering

Essentials

- Factor VIIa (FVIIa) is an allosteric enzyme responsible for blood coagulation initiation.
- We developed a fully inhibitory antibody (mAb4F5) against a superactive FVIIa analogue ($FVIIa_{DVQ}$).
- We characterized and solved the crystal structure of the Fab fragment (Fab4F5).
- Molecular docking and small-angle X-ray scattering helped building the $FVIIa_{DVQ}$:Fab4F5 complex.

1 | INTRODUCTION

Blood clotting is preventing blood loss as well as infiltration of microbes. Factor VIIa (FVIIa) is one key enzyme in the initiation phase of the coagulation cascade,[1,2] forming a complex with tissue factor (TF) exposed upon injury. The role of TF is to promote FVII conversion to FVIIa by localization as well as to convert zymogen-like FVIIa to the active conformation and make it an efficient catalyst of FVII, factor X, and factor IX activation.[3] Attempts at creating less TF-dependent FVIIa variants, that is, molecules with a built-in stabilization of the active conformation and elevated intrinsic enzymatic activity, have among other variants given rise to V21D/E154V/M156Q-FVIIa ($FVIIa_{DVQ}$, chymotrypsinogen numbering).[4]

Analogue $FVIIa_{DVQ}$ was originally developed with the aim of offering a more potent FVIIa-based treatment of hemophilia.[5] Even though it proved very efficacious in the clinical trials,[6] $FVIIa_{DVQ}$ provoked the immune system in some patients, and the clinical trials were terminated due to the detection of antidrug antibodies.[7] $FVIIa_{DVQ}$ was more proteolytically active compared to FVIIa, even though it can be further stimulated by TF, retained the substrate specificity of FVIIa, and efficiently promoted thrombin and fibrin generation.[4,8] The need for a monoclonal antibody that could be used to quantify $FVIIa_{DVQ}$ in clinical samples also containing endogenous FVII(a) led to the identification of mAb4F5. This antibody also turned out to be a powerful tool for studying FVIIa allostery.

In this study, we characterized mAb4F5 binding to $FVIIa_{DVQ}$, which is of very high affinity (K_d <100 pmol/L), and its functional consequences. We have determined the crystal structure of the Fab fragment of mAb4F5 (Fab4F5) and described the potential antigen-combining sites. We used molecular docking, restrained by experimental small-angle X-ray scattering (SAXS), to build a model of the $FVIIa_{DVQ}$:Fab4F5 complex, which possessed considerable stability. The binary complex explains and supports the unique selectivity and, in an allosteric context, functional consequences of Fab4F5 association with $FVIIa_{DVQ}$.

2 | MATERIALS AND METHODS

2.1 | Expression and purification of $FVIIa_{DVQ}$ and Fab4F5 and activity measurements

The FVIIa variants ($FVIIa_{DVQ}$, $FVIIa_{DV}$, $FVIIa_{DQ}$ and $FVIIa_{VQ}$) were expressed and purified as described previously,[4,9,10] $FVIIa_{DVQ}$ was inhibited by incubation with D-Phe-Phe-Arg chloromethylketone (fFR-ck),[11] and mAb4F5 was generated by standard hybridoma technology after immunizing mice with $FVIIa_{DVQ}$. To produce the Fab fragment of mAb4F5 (Fab4F5), the antibody was digested with papain in 15 mmol/L cysteine with 2 mmol/L EDTA for 6 hours at 37°C at an enzyme-to-antibody ratio of 1:100 (w/w). Fab4F5 was purified from the digestion by protein A affinity chromatography in phosphate-buffered saline followed by cation-exchange chromatography (GE Healthcare MonoS 5/50 GL) in 25 mmol/L acetate, pH 5.5.

Purified Fab4F5 was dialyzed in 20 mmol/L Tris-HCl, pH 7.4, overnight and concentrated to about 10 mg/mL using stirred ultrafiltration cells (Millipore and Amicon Bioseparations, Model-5124) for crystallization. The purity and homogeneity of the protein were confirmed by reduced SDS-PAGE and analytical gel filtration.

The enzymatic activity of 20 nmol/L $FVIIa_{DVQ}$ in the absence and presence of 100 nmol/L mAb4F5 was measured in 50 mmol/L HEPES, pH 7.4, containing 0.1 mol/L NaCl, 5 mmol/L $CaCl_2$, 0.1% (w/v) bovine serum albumin, using 1 mmol/L S-2288 (Chromogenix, Milan, Italy).

2.2 | Characterization of FVIIa variant binding to mAb4F5 by surface plasmon resonance (SPR)

The binding analyses were run on a Biacore 3000 instrument (Biacore AB, Uppsala, Sweden) at 25°C. Antimouse IgG1, 30 μg/mL in 10 mmol/L sodium acetate, pH 5.0, was immobilized onto a CM5 sensor chip using amine coupling chemistry and used throughout the whole series. The flow rate was 5 μL/min and the injection time 7 minutes. Each subsequent binding experiment comprised the initial capture of mAb4F5 by the antimouse IgG1, followed by the binding of FVIIa variants (1-50 nmol/L) to mAb4F5 at a flow rate of 20 μL/min. The running buffer was 20 mmol/L HEPES, pH 7.4, 100 mmol/L NaCl, 2 mmol/L $CaCl_2$, 0.005% (v/v) surfactant (P20). The chip was regenerated with 10 mmol/L glycine, pH 1.7, between each run. Binding kinetics were evaluated using BIAevaluation 4.1 software.

2.3 | Crystallization and Data Collection

Crystallizations of Fab4F5 were performed using the sitting drop vapor diffusion method in 48-well plates. Typically, 1 μL protein solution was mixed with an equal volume of screening solution and equilibrated over 100 μL of the latter in the reservoir. Initial screens were carried out with Hampton Research Screen Kits (Hampton Research, Aliso Viejo, CA) at room temperature. Large single crystals were obtained when a 1.5-μL protein droplet was mixed with an equal volume of reservoir solution consisting of 2.3 mol/L ammonium sulfate, 100 mmol/L Tris-HCl, pH 7.4, 5% (w/v) PEG400. The crystals appeared in about 2 days.

X-ray diffraction data of Fab4F5 was collected at the BL17U beamline, Shanghai Synchrotron Radiation Facility. Prior to mounting on the X-ray machine, the crystals were dipped briefly in the mother liquor containing 20% glycerol (v/v) as a cryoprotectant. All diffraction data were indexed and processed by the HKL2000 software package (HKL Research, Charlottesville, VA).[12] The crystal belonged to the space group I23 with cell dimension a = 141.64 Å, b = 141.64 Å, c = 141.64 Å. A crystallographic asymmetric unit contained 2 molecules. Statistics of data collection are reported in Table 1.

2.4 | Crystal structure determination and refinement

The structure of Fab4F5 was solved by molecular replacement[13] using the light chain of the Fab fragment of MN20B9.34 anti-P1.4 antibody (PDB code: 2BRR)[14] and the heavy chain of the Fab fragment of β2 adrenoceptor antibody (PDB code: 2R4R)[15] as the search models. The structure was refined by CCP4[13] without noncrystallographic symmetry restraints. The $2F_o$–F_c and F_o–F_c electron density maps were examined, and the protein model was manually adjusted after each refinement cycle using the molecular graphics program COOT.[16] Solvent molecules were added using an F_o–F_c map contoured at 2.5 σ in the final refinement step. The majority of residues in the final model have allowed stereochemistry in a Ramachandran plot as shown by PROCHECK.[17] The final model refinement statistics are summarized in Table 1. The structure was analyzed by PyMOL.[18]

TABLE 1 X-ray data collection and model refinement statistics for Fab4F5 structure

Crystals	Fab4F5
Data collection	
X-ray wavelength (Å)	1.0
Resolution limits (Å)	1.81
Space group	I23
Cell parameters (Å)	a = 141.64, b = 141.64, c = 141.64, α = 90°, β = 90°, γ = 90°
Temperature of experiments (K)	100
Completeness (%)	100
Redundancy	29.3 (30)[a]
Average I/σ	25.9 (2.4)[a]
Rmerge[b]	0.082 (1.8)[a]
Refinement data	
R-factor	0.209
R-free	0.247
Average B-factor (Å^2) of protein	36.6
r.m.s deviation of bond lengths (Å)	0.009
r.m.s deviation of bond angle (°)	1.312
Ramachandran analysis (%)	95.5[c], 3.8[d], 0.7[e]

[a]Numbers in parentheses refer to the highest resolution shells.
[b]Rmerge = Σ|Ii-<I>|/ΣIi, where Ii is the intensity of the ith observation and <I> is the mean intensity of the reflections.
[c]Percentage of residues in most favored regions.
[d]Percentage of residues in additional allowed regions.
[e]Percentage of residues in generously allowed regions.

2.5 | Molecular modeling and refinement

Molecular modeling of the $FVIIa_{DVQ}$: Fab4F5 structure was carried out by the program HADDOCK.[19] A molecular model of $FVIIa_{DVQ}$ was generated and mutated from the crystal structure of FVII zymogen (epidermal growth factor [EGF]2/protease domains) in complex with inhibitory exosite peptide A-183 (PDB code: 1JBU).[20] FVIIa residues previously found to be important for Fab4F5 interactions (Table 2) were defined as the constraints. The molecular models generated by HADDOCK were grouped into 7 clusters based on the structural similarities, and the cluster with the lowest energy had 54 members. This cluster satisfied most interaction restraints and showed the largest buried interface area of approximately 877 Å^2 between Fab4F5 and $FVIIa_{DVQ}$. The model was then subjected to further refinement by CNS model minimization protocol.

2.6 | SAXS and structural modeling of $FVIIa_{DVQ}$:Fab4F5

$FVIIa_{DVQ}$:Fab4F5 complex solution scattering data was collected at the SAXS beamline (BL19U2) of National Center for Protein Science Shanghai. Samples were further purified by gel filtration in the SAXS experimental buffer (20 mmol/L Tris-HCl, 150 mmol/L NaCl, pH 7.4). All data sets were collected with an exposure time of 1 second at 283 K. Three different concentrations (1, 3, and 6 mg/mL) of the protein were used for the measurements.

Scattering data for buffer used for subtractions were collected between every 2 protein samples. Multiple curves with different concentrations and exposure times were scaled and merged to generate an ideal average scattering curve. The qualities of the scattering curves were examined by the program PRIMUS[21] to ensure that there was no obvious aggregation and radiation damage before further analysis. The initial R_g values were calculated from the Guinier plot, and only data from low q values were used for the calculation. The P(r) distribution function was calculated with the program GNOM.[20]

TABLE 2 Kinetics of interactions between mAb4F5 and various FVIIa variants derived from SPR measurements

FVIIa variants	K_{on} (×10^5 per mol/L/s)	K_{off} (× 10^{-5} per s)	K_d (nmol/L)
FVIIa	0.35	530	150
$FVIIa_{DVQ}$	2.1	0.68	0.032
$FVIIa_{DV}$	1.4	16	1.1
$FVIIa_{DQ}$	1.3	24	1.9
$FVIIa_{VQ}$	0.27	350	130
K20E-$FVIIa_{DVQ}$	1.0	1000	100

The low-resolution shapes of the protein in solution were modeled by the program DAMMIF[22] in P1 symmetry, which performed 20 individual calculations. Subsequently, continuous and meaningful shapes were collected and averaged by DAMAVER.[23] The starting model of $FVIIa_{DVQ}$ was extracted from PDB entry 1JBU,[20] and the EGF domains of PDB entry 1QFK[24] were used as an additional protein domain. The solved crystal structure of Fab4F5 was used as the model of Fab4F5 (PDB code: 5YUP). The complex model was then refined by the CNS v1.2 package.[25]

3 | RESULTS AND DISCUSSION

3.1 | V21D, 1 of the 3 mutations in $FVIIa_{DVQ}$, is pivotal for recognition by mAb4F5

SPR experiments used to characterize the binding of mAb4F5 to $FVIIa_{DVQ}$ showed that mAb4F5 specifically recognized 1 of the 3 mutations in $FVIIa_{DVQ}$. The binding of $FVIIa_{DVQ}$, $FVIIa_{DV}$, $FVIIa_{DQ}$, and $FVIIa_{VQ}$ to mAb4F5 were compared, and the V21D mutation turned out a prerequisite for high-affinity (picomolar) mAb4F5 binding of $FVIIa_{DVQ}$ (Table 2). However, all 3 mutations were required for optimal affinity. Regular FVIIa was only weakly recognized by mAb4F5. Furthermore, it was evident that K20E-$FVIIa_{DVQ}$ was poorly recognized by mAb4F5. Thus, residues Lys20 and Asp21 in $FVIIa_{DVQ}$ were crucial components of the epitope for mAb4F5. Interestingly, mAb4F5 did not recognize $FVIIa_{DVQ}$ after inhibition with fFR-ck, supporting an allosteric linkage between the active site and the N-terminal tail of the protease domain, which ensures burial of the tail upon inhibitor incorporation and makes residue 21 inaccessible for antibody binding.

The binding of mAb4F5 to $FVIIa_{DVQ}$ eliminated >99% of the amidolytic enzyme activity, whereas the activity of FVIIa was unaffected by the presence of mAb4F5. This is in line with the hypothesis that mAb4F5 binding to its epitope, comprising at least 2 residues close to the tail N-terminus (Ile16), prevents tail insertion into the activation pocket. $FVIIa_{DVQ}$ is in a conformational equilibrium between an active form with the N-terminus inserted into the activation pocket and a latent form with an exposed N-terminal tail. Conceivably, mAb4F5 grabs hold of its epitope when exposed and accessible and thereby prevents tail reinsertion and precludes $FVIIa_{DVQ}$ enzymatic activity. In other words, mAb4F5 binding locks $FVIIa_{DVQ}$ in the zymogen-like conformation with a truly "homeless" N-terminus.

3.2 | Crystal structure of Fab fragment of mAb4F5

The crystal structure of Fab4F5 was solved with the molecular replacement method and refined to high resolution (1.81 Å) with an R factor of 20.9% and a R_{free} factor of 24.7% (Table 1). There were 2 Fab4F5 molecules in the asymmetric unit, corresponding to a Matthews coefficient of 2.39 A^3/Da and a solvent content of 48.6%. The average temperature factor for Fab4F5 was 36.6 Å. This structure had a good stereochemical geometry with the root mean square deviation values for bond lengths of 0.009 Å and for bond angles 1.3°. In addition, 99.3% of the residues were in the allowed region of the Ramachandran plot (Table 1).

The Fab4F5 structure has the typical immunoglobulin fold consisting of V_L and C_L domains of the light chain and V_H and C_H domains of the heavy chain, with elbow angles of 136.7°. The conformation of the Fab4F5 CDRs is well defined even though no antigen is bound at the combining site. Three CDRs are found on the light chain (L1-L3) and 3 on the heavy chain (H1-H3) (Figure 1). Among them, the length of H2 (15 residues) in Fab4F5 is shorter than the usual length (16-19 residues) seen in other Fab variants.[26,27] There is a long groove about 15.6 Å wide including 1 hydrophobic pocket (Leu96L, Kabat numbering) and 1 charged pocket (Asp95H and Tyr99H). These 2 pockets plus Tyr98H presumably constitute the antigen-binding sites (Figure 2).

3.3 | Docking analysis of interactions between $FVIIa_{DVQ}$ and Fab4F5

A crystal structure of $FVIIa_{DVQ}$ in complex with Fab4F5 would be ideal to understand in detail the molecular interactions between the 2 proteins. Unfortunately, the crystallization of such a complex failed despite numerous trials (using Gla-domainless $FVIIa_{DVQ}$ obtained by digestion with cathepsin G). However, the availability of the current Fab4F5 structure and a published crystal structure of FVII in its zymogen form[20] allowed us to build a molecular model of the $FVIIa_{DVQ}$:Fab4F5 complex using the protein-protein docking program HADDOCK.[19]

HADDOCK allows the use of the constraints identified from mutagenesis studies during the molecular docking. On the $FVIIa_{DVQ}$ side, we identified residues Lys20 and Asp21 as the key residues for Fab4F5 interaction. On the Fab4F5 side, the CDR loops are the typical antigen-combining site. The heavy-chain H3 loop of antibodies is typically the most important for antigen recognition.[28] The CDR H3 loop of Fab4F5 has 9 residues, which is the typical length of H3 loops for antiprotein antibodies.[29] This length is the same as that of Fab112, which binds to the autolysis loop of urokinase-type plasminogen activator.[30] In contrast to Fab4F5, an antimatriptase antibody (FabE2, PDB code: 3BN9) has a very long H3 loop (18 residues), which inserts into the canyon-like active site cleft and occupies the subsite pockets (S1-S4).[31] Therefore, the length of the CDR H3 loop of mAb4F5 suggests that the H3 most likely does not bind to the active site of $FVIIa_{DVQ}$. Tyrosine is the most prominent type of amino acid residue involved in the mAb4F5-$FVIIa_{DVQ}$ interaction. This is a feature commonly found in the interface between an antibody and its macromolecular antigen.[32] As noted previously, the side chain of tyrosine is large enough to occupy large volumes of space with only a few torsion angles, and it can also form hydrogen bonds, hydrophobic interactions, and attractive electrostatic interactions with positively charged groups. Moreover, the uncharged side chain of tyrosine avoids electrostatic repulsion effects, and its midrange hydrophilicity allows it to adapt favorably to both hydrophilic and hydrophobic environments.[33,34] Thus, we docked Fab4F5 as determined in this work onto $FVIIa_{DVQ}$ based on the shapes and charges

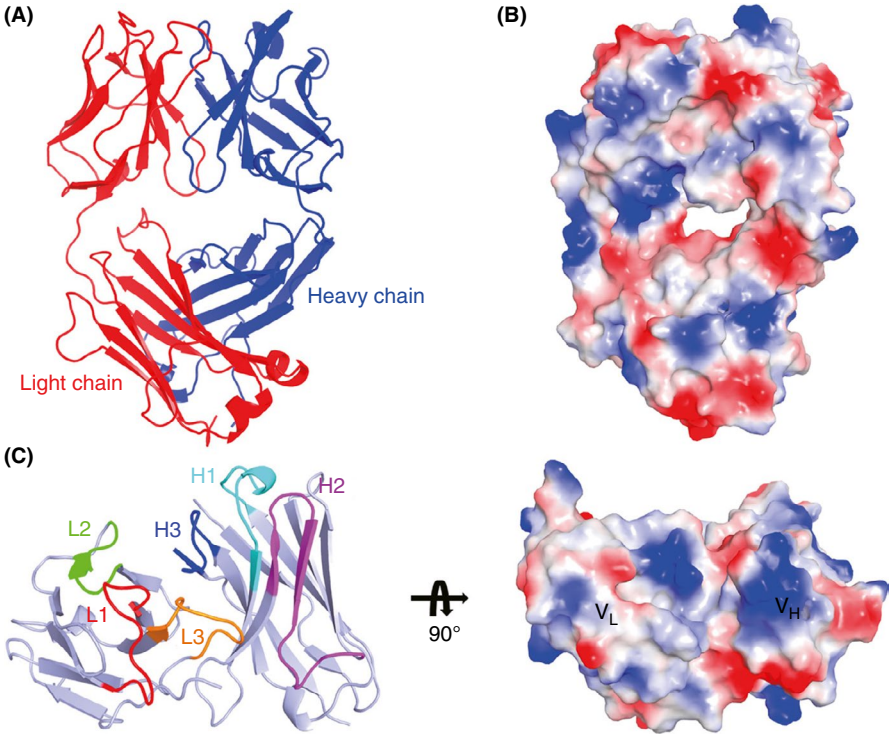

FIGURE 1 Crystal structure of Fab fragment of mAb4F5. (A) Overall structure of Fab4F5; (B) The electrostatic potential surface of Fab4F5; (C) Structure showing the CDR regions of Fab4F5 (colored loops on the left panel) forming an undulated surface, a typical feature of an antiprotein antibody. The CDR loops are colored, with L1 in red, L2 in green, L3 in orange, H1 in blue, H2 in magenta, and H3 in cyan, and the framework region in light blue. The electrostatic potential surface of the variable region of Fab4F5 is shown in the right panel from a top view

of their molecular surfaces, constrained by the direct interactions between the $FVIIa_{DVQ}$ and the CDR H3 loop (Tyr98H and Tyr99H).[35]

In the resulting molecular model of $FVIIa_{DVQ}$:Fab4F5 complex, Fab4F5 is involved in extensive interactions mainly with the tail of the protease domain of $FVIIa_{DVQ}$, where the N-terminal part (Lys20 and Asp21) is grabbed by the CDR H3 loop (Figure 3). On the antibody side, the heavy chains dominate antigen recognition, which is the typical case in many antibody- antigen complexes.[28] Two tyrosine residues (Tyr98H and Tyr99H) from the CDR H3 loop are key residues for $FVIIa_{DVQ}$ binding by making hydrogen bonds with the tail residues Lys20 and Asp21. This way, mAb4F5 may prevent the liberated N-terminus of the activation loop from inserting into the activation pocket and thus retain $FVIIa_{DVQ}$ in the zymogen-like conformation.

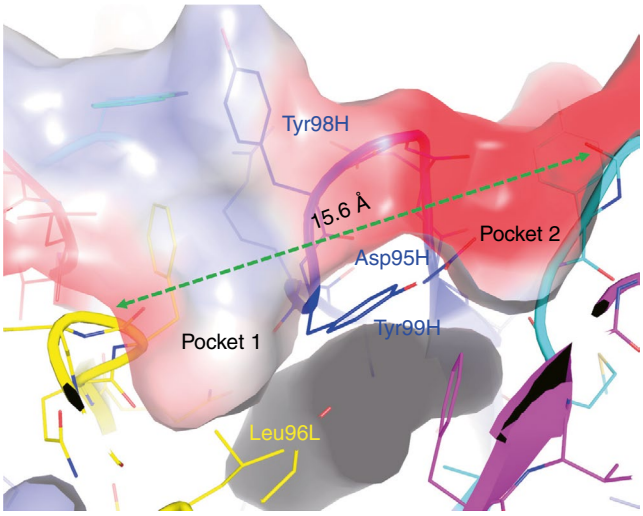

FIGURE 2 Antigen-binding pockets in the CDR regions of Fab4F5. Fab4F5 contains a long groove about 15.6 Å wide, including one hydrophobic pocket (pocket 1) and one charged pocket (pocket 2). CDR, complementarity-determining region

3.4 | SAXS structure shows that $FVIIa_{DVQ}$ interacts with Fab4F5 to form a stable complex in solution

We next used SAXS to model the 3-dimensional structure of the $FVIIa_{DVQ}$:Fab4F5 complex. The complex was assembled using a 2-fold molar excess of Fab4F5 and purified by gel filtration chromatography in a buffer (50 mmol/L Tris, 150 mmol/L NaCl, pH 7.4). We observed that $FVIIa_{DVQ}$:Fab4F5 was a monomer on a Superdex 200 10/300 GL column with a retention volume of about 13.4 mL, which is consistent with the complex's estimated molecular mass of 84 kDa. The scattering data were collected from the sample of 3 mg/mL (Figure 4A), which showed no radiation damage and higher signal-to-noise ratio. The clear linear behavior of the Guinier plot also strongly suggested that $FVIIa_{DVQ}$:Fab4F5 is a monodisperse protein (inset of Figure 4A), and its radius of gyration (R_g) is 40.2 Å. According to Kratky analysis, there is a peak with a height of around 9.8 at low q values, which returns to zero at high q values, but at a slower rate than expected from compact proteins. This indicates an intact, folded conformation of $FVIIa_{DVQ}$:Fab4F5 with some flexibility in solution (Figure 4B).

To reconstruct the molecular envelope of the $FVIIa_{DVQ}$:Fab4F5 complex from the scattering curve, it is important to know whether molecular symmetry is present in the particle. As mentioned previously, the retention volume of $FVIIa_{DVQ}$:Fab4F5 showed that this complex was monomeric. Thus, we reconstructed the

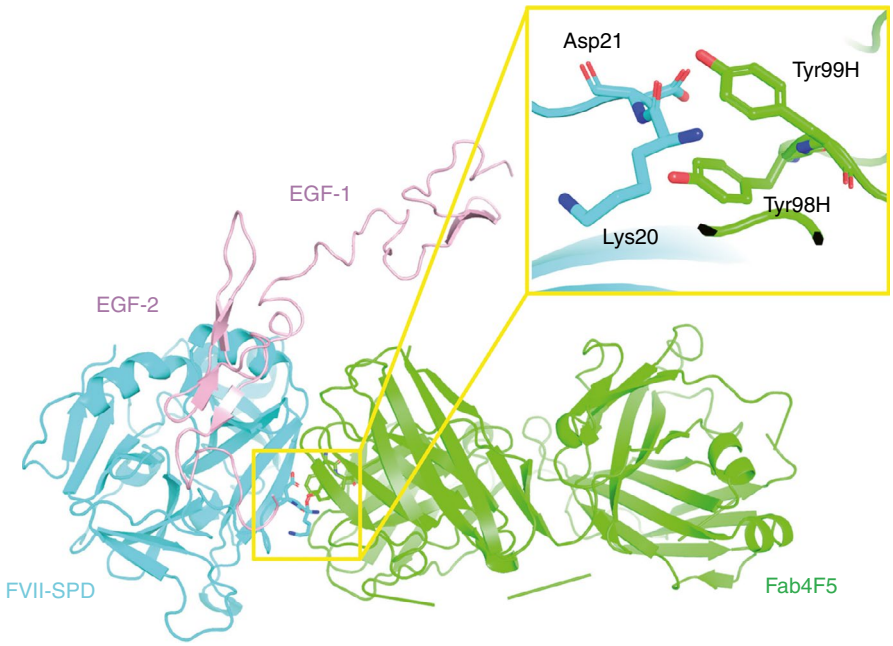

FIGURE 3 Docking model of $FVIIa_{DVQ}$:Fab4F5. The N-terminal tail of the protease domain (Lys20 and Asp21) is grabbed by Tyr98H and Tyr99H of Fab4F5's CDR H3 loop. CDR, complementarity-determining region; EGF, epidermal growth factor

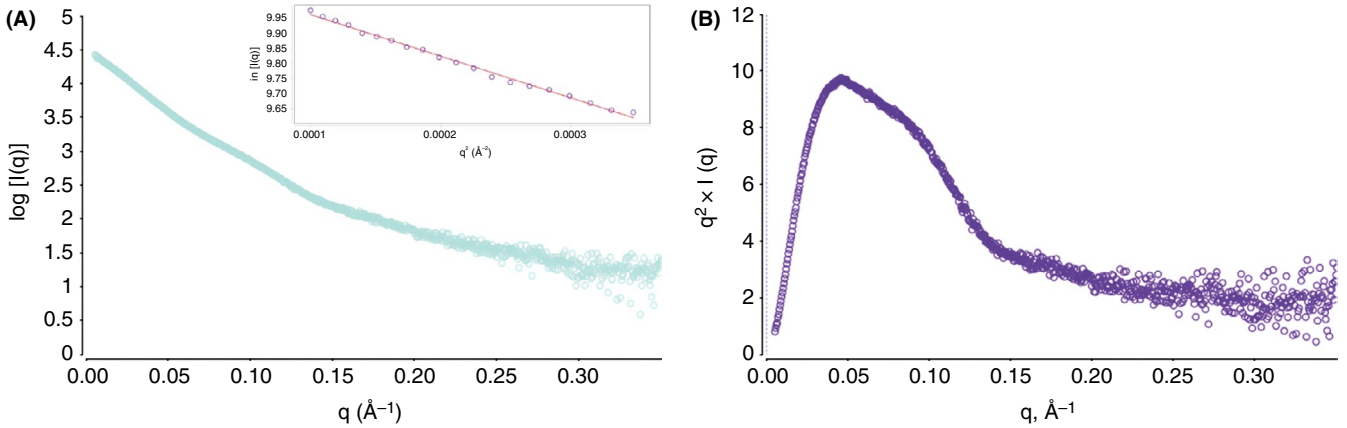

FIGURE 4 SAXS data of $FVIIa_{DVQ}$:Fab4F5. (A) Experimental SAXS of $FVIIa_{DVQ}$: Fab4F5 in solution. The Guinier region and the corresponding linear fitting are shown in the inset. (B) Kratky plot calculated from the experimental data. Bell-shaped curves indicate compact structures. EGF, epidermal growth factor; SAXS, small-angle X-ray scattering

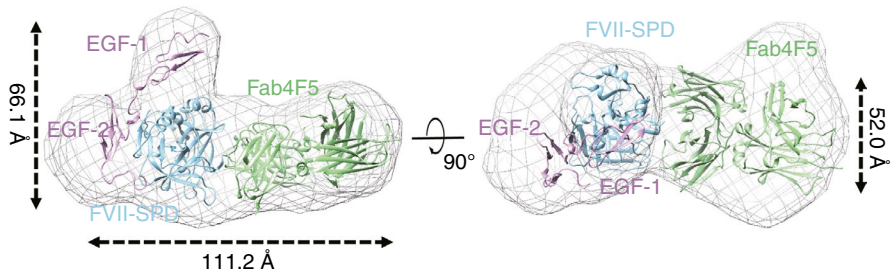

FIGURE 5 SAXS structure showing that $FVIIa_{DVQ}$ forms a stable complex with Fab4F5 in solution. Superposition of the experimental envelope (shown as a mesh) onto the predicted $FVIIa_{DVQ}$: Fab4F5 structure represented as a cartoon with monomer chains shown in different colors. EGF, epidermal growth factor; SAXS, small-angle X-ray scattering

$FVIIa_{DVQ}$:Fab4F5 molecular envelope using the program DAMMIF with P1 symmetry.[36] We used DAMAVER to generate the averaged molecular envelope.[23] The model was then generated based on the docking results and built into the averaged molecular envelope of the $FVIIa_{DVQ}$:Fab4F5 using the program CHIMERA.[37] In the overall structure, the $FVIIa_{DVQ}$:Fab4F5 complex envelope

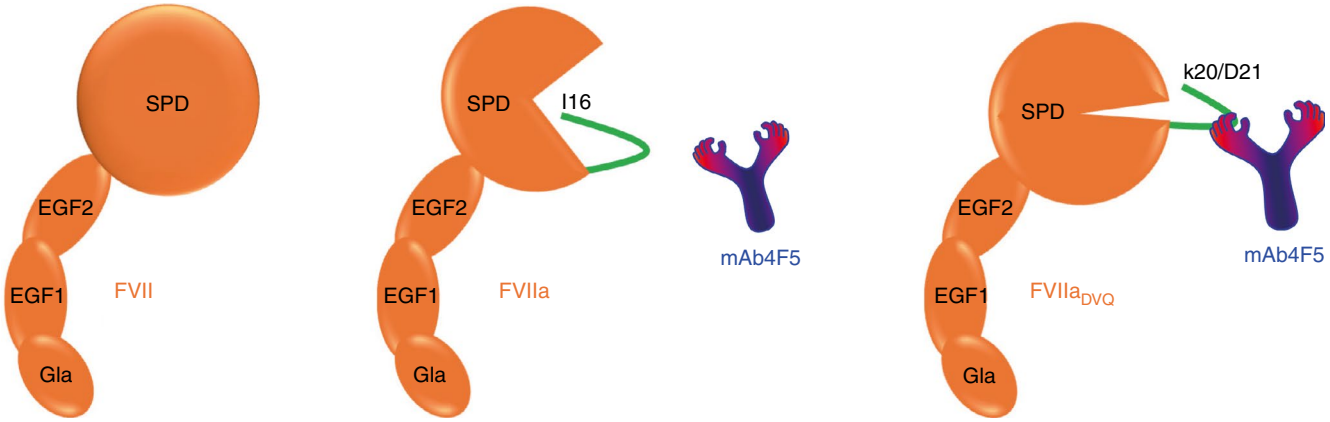

FIGURE 6 Schematic representation of the inhibitory mechanism of mAb4F5. mAb4F5 prevents the liberated N-terminus of the activation loop from inserting into the activation pocket and thereby keeps FVIIa$_{DVQ}$ in the zymogen-like conformation, Lys20 and Asp21 in FVIIa$_{DVQ}$ are pivotal for high-affinity recognition by mAb4F5. EGF, epidermal growth factor; SPD, serine protease domain

has an irregular cylinder shape with a dimension of approximately 111.2 Å × 52.0 Å × 66.1 Å (Figure 5).

Although the SAXS model has limited resolution (20 Å) and cannot reveal the conformation of individual residues, this low-resolution model is consistent with all available data, and clearly demonstrates that Fab4F5 binds to FVIIa$_{DVQ}$ and forms a stable complex structure in solution. In this complex, we modeled 3 domains of FVIIa$_{DVQ}$, including EGF-1, EGF-2, and serine protease domain. There still exists some unpopulated SAXS density in the resulting model presumably due to interdomain flexibility. The exposed N-terminus of the FVIIa protease domain, together with β-sheets of the enzyme, contribute to the interaction with the CDRs of Fab4F5 (interface area 877.4 Å^2 as calculated by PISA[38]).

In conclusion, our biochemical and biophysical data show that the inhibition mechanism of mAb4F5. mAb4F5 captures the liberated N-terminus of the activation loop of FVIIa$_{DVQ}$ and prevents it from inserting into the activation pocket, thereby keeping FVIIa$_{DVQ}$ in the latent, zymogen-like conformation (Figure 6).

4 | PROTEIN DATA BANK ACCESSION NUMBER

The coordinate of the Fab4F5 structure has been deposited in the Protein Data Bank (PDB code: 5YUP).

ACKNOWLEDGMENTS

This study was supported by grants from National Key R&D Program of China (2017YFE0103200), Novo Nordisk-Chinese Academy of Science Research Foundation (NNCAS-2012-5(A)), National Natural Science Foundation of China (31400637, 31161130356, 31170707 and 31370737) and Fujian province (2018J01729). We thank the staffs from the BL17U and BL19U2 beamline at Shanghai Synchrotron Radiation Facility for assistance during data collection.

RELATIONSHIP DISCLOSURE

The authors report nothing to disclose.

AUTHOR CONTRIBUTIONS

LJ was involved in protein preparation, crystallization, structure determination, and analysis; XX participated in SAXS structure analysis. JL participated in molecular docking and analysis. EP prepared proteins, performed and analyzed the cleavage rate and binding experiments, and participated in the preparation of the manuscript; EP and MH has led the project and finalized the manuscript.

ORCID

Egon Persson https://orcid.org/0000-0003-3005-4926

REFERENCES

1. Davie EW, Fujikawa K, Kisiel W. The coagulation cascade: initiation, maintenance, and regulation. Biochemistry. 1991;30:10363–70.
2. Long AT, Kenne E, Jung R, Fuchs TA, Renne T. Contact system revisited: an interface between inflammation, coagulation, and innate immunity. J Thromb Haemost. 2016;14:427–37. https://doi.org/10.1111/jth.13235.
3. Banner DW, D'Arcy A, Chene C, Winkler FK, Guha A, Konigsberg WH, et al. The crystal structure of the complex of blood coagulation factor VIIa with soluble tissue factor. Nature. 1996;380:41–6.
4. Persson E, Kjalke M, Olsen OH. Rational design of coagulation factor VIIa variants with substantially increased intrinsic activity. Proc Natl Acad Sci. 2001;98:13583–8.
5. Persson E, Olsen OH, Bjorn SE, Ezban M. Vatreptacog alfa from conception to clinical proof of concept. Semin Thromb Hemost. 2012;38:274–81.
6. Lentz SR, Ehrenforth S, Karim FA, Matsushita T, Weldingh KN, Windyga J, et al. ; adept™2 Investigators. Recombinant factor VIIa analog in the management of hemophilia with inhibitors: results from a multicenter, randomized, controlled trial of vatreptacog alfa. J Thromb Haemost. 2014;12:1244–53.

7. Mahlangu JN, Weldingh KN, Lentz SR, Kaicker S, Karim FA, Matsushita T, et al. ; adept™2 Investigators. Changes in the amino acid sequence of the recombinant human factor VIIa analog, vatreptacog alfa, are associated with clinical immunogenicity. J Thromb Haemost. 2015;13:1989–98.
8. Sorensen B, Persson E, Ingerslev J. Factor VIIa analogue (V158D/E296V/M298Q-FVIIa) normalises clot formation in whole blood from patients with severe haemophilia A. Br J Haematol. 2007;137:158–65.
9. Persson E, Bak H, Olsen OH. Substitution of valine for leucine 305 in factor VIIa increases the intrinsic enzymatic activity. J Biol Chem. 2001;276:29195–9.
10. Persson E, Nielsen LS, Olsen OH. Substitution of aspartic acid for methionine-306 in factor VIIa abolishes the allosteric linkage between the active site and the binding interface with tissue factor. Biochemistry. 2001;40:3251–6.
11. Sorensen BB, Persson E, Freskgard PO, Kjalke M, Ezban M, Williams T, et al. Incorporation of an active site inhibitor in factor VIIa alters the affinity for tissue factor. J Biol Chem. 1997;272:11863–8.
12. Otwinowski Z, Minor W. Processing of X-ray diffraction data collected in oscillation mode. Methods Enzymol. 1997;276:307–26.
13. Collaborative Computational Project, Number 4. The CCP4 suite: programs for protein crystallography. Acta Crystallogr D Biol Crystallogr. 1994;50:760–3.
14. Oomen CJ, Hoogerhout P, Kuipers B, Vidarsson G, van Alphen L, Gros P. Crystal structure of an Anti-meningococcal subtype P1.4 PorA antibody provides basis for peptide-vaccine design. J Mol Biol. 2005;351:1070–80.
15. Rasmussen SG, Choi HJ, Rosenbaum DM, Kobilka TS, Thian FS, Edwards PC, et al. Crystal structure of the human beta2 adrenergic G-protein-coupled receptor. Nature. 2007;450:383–7.
16. Emsley P, Cowtan K. Coot: model-building tools for molecular graphics. Acta Crystallogr D Biol Crystallogr. 2004;60:2126–32.
17. Laskowski RA, Macarthur MW, Moss DS, Thornton JM. PROCHECK: a program to check the stereochemical quality of protein structures. J Appl Crystallogr. 1993;26:283–91.
18. Delano WL. The PyMOL molecular graphics system, Version 2.0 Schrödinger, LLC; 2002.
19. van Zundert GCP, Rodrigues J, Trellet M, Schmitz C, Kastritis PL, Karaca E, et al. The HADDOCK2.2 web server: user-friendly integrative modeling of biomolecular complexes. J Mol Biol. 2016;428:720–5.
20. Eigenbrot C, Kirchhofer D, Dennis MS, Santell L, Lazarus RA, Stamos J, et al. The factor VII zymogen structure reveals reregistration of beta strands during activation. Structure. 2001;9:627–36.
21. Konarev PV, Volkov VV, Sokolova AV, Koch MHJ, Svergun DI. PRIMUS: a Windows PC-based system for small-angle scattering data analysis. J Appl Crystallogr. 2003;36:1277–82.
22. Mertens HD, Svergun DI. Structural characterization of proteins and complexes using small-angle X-ray solution scattering. J Struct Biol. 2010;172:128–41.
23. Volkov VV, Svergun DI. Uniqueness of ab initio shape determination in small-angle scattering. J Appl Crystallogr. 2003;36:860–4.
24. Pike AC, Brzozowski AM, Roberts SM, Olsen OH, Persson E. Structure of human factor VIIa and its implications for the triggering of blood coagulation. Proc Natl Acad Sci U S A. 1999;96:8925–30.
25. Brunger AT. Version 1.2 of the Crystallography and NMR system. Nat Protoc. 2007;2:2728–33. https://doi.org/10.1038/nprot.2007.406.
26. Collis AV, Brouwer AP, Martin AC. Analysis of the antigen combining site: correlations between length and sequence composition of the hypervariable loops and the nature of the antigen. J Mol Biol. 2003;325:337–54.
27. Almagro JC. Identification of differences in the specificity-determining residues of antibodies that recognize antigens of different size: implications for the rational design of antibody repertoires. J Mol Recognit. 2004;17:132–43.
28. Ganesan R, Eigenbrot C, Kirchhofer D. Structural and mechanistic insight into how antibodies inhibit serine proteases. Biochem J. 2010;430:179–89.
29. Wu TT, Johnson G, Kabat EA. Length distribution of CDRH3 in antibodies. Proteins. 1993;16:1–7.
30. Jiang L, Botkjaer KA, Andersen LM, Yuan C, Andreasen PA, Huang M. Rezymogenation of active urokinase induced by an inhibitory antibody. Biochem J. 2013;449:161–6.
31. Farady CJ, Egea PF, Schneider EL, Darragh MR, Craik CS. Structure of an Fab-protease complex reveals a highly specific non-canonical mechanism of inhibition. J Mol Biol. 2008;380:351–60.
32. Fellouse FA, Wiesmann C, Sidhu SS. Synthetic antibodies from a four-amino-acid code: a dominant role for tyrosine in antigen recognition. Proc Natl Acad Sci U S A. 2004;101:12467–72.
33. Zemlin M, Klinger M, Link J, Zemlin C, Bauer K, Engler JA, et al. Expressed murine and human CDR-H3 intervals of equal length exhibit distinct repertoires that differ in their amino acid composition and predicted range of structures. J Mol Biol. 2003;334:733–49.
34. Mian IS, Bradwell AR, Olson AJ. Structure, function and properties of antibody binding sites. J Mol Biol. 1991;217:133–51.
35. Blouse GE, Botkjaer KA, Deryugina E, Byszuk AA, Jensen JM, Mortensen KK, et al. A novel mode of intervention with serine protease activity: targeting zymogen activation. J Biol Chem. 2009;284:4647–57.
36. Franke D, Svergun DI. DAMMIF, a program for rapid ab-initio shape determination in small-angle scattering. J Appl Crystallogr. 2009;42:342–6.
37. Pettersen EF, Goddard TD, Huang CC, Couch GS, Greenblatt DM, Meng EC, et al. UCSF Chimera–a visualization system for exploratory research and analysis. J Comput Chem. 2004;25:1605–12.
38. Krissinel E, Henrick K. Inference of macromolecular assemblies from crystalline state. J Mol Biol. 2007;372:774–97.

How to cite this article: Jiang L, Xie X, Li J, Persson E, Huang M. Crystal structure, epitope, and functional impact of an antibody against a superactive FVIIa provide insights into allosteric mechanism. *Res Pract Thromb Haemost*. 2019;3:412–419. https://doi.org/10.1002/rth2.12211